

# Temporally Coherent Embeddings for Self-Supervised Video Representation Learning

Joshua Knights<sup>1</sup>, Anthony Vanderkop<sup>1,2</sup>, Daniel Ward<sup>1,3</sup>, Olivia Mackenzie-Ross<sup>1,3</sup>, and Peyman Moghadam<sup>1,2</sup>

<sup>1</sup> CSIRO-Data61, Brisbane, QLD 4069, Australia

<sup>2</sup> Queensland University of Technology (QUT), Brisbane, QLD 4000, Australia

<sup>3</sup> The University of Queensland (UQ), Brisbane, QLD 4072, Australia

{firstname.lastname}@csiro.au

**Abstract.** This paper presents *TCE*: *Temporally Coherent Embeddings* for self-supervised video representation learning. The proposed method exploits inherent structure of unlabeled video data to explicitly enforce temporal coherency in the embedding space, rather than indirectly learning it through ranking or predictive *pretext* tasks. In the same way that high-level visual information in the world changes smoothly, we believe that nearby frames in learned representations should demonstrate similar properties. Using this assumption, we train the *TCE* model to encode videos such that adjacent frames exist close to each other and videos are separated from one another. Using *TCE* we learn robust representations from large quantities of unlabeled video data. We evaluate our self-supervised trained *TCE* model by adding a classification layer and finetuning the learned representation on the downstream task of video action recognition on the UCF101 dataset. We obtain 68.7% accuracy and outperform the state-of-the-art self-supervised methods despite using a significantly smaller dataset for pre-training. Notably, we demonstrate results competitive with more complex 3D-CNN based networks while training with a 2D-CNN network backbone on action recognition tasks.

## 1 Introduction

Many state of the art image and video deep learning approaches have heavily relied on fully-supervised methods along with the abundance of manually annotated datasets. However obtaining labels for many tasks is impractical and not scalable, especially when considering the ambiguities in complex data sources such as videos or point clouds.

Self-Supervised Learning (SSL) is a new and promising paradigm, where a model is trained on unlabeled data based on a learning signal constructed from inherent structure in the training sample. With SSL it is possible to leverage enormous amounts of unlabeled data to learn robust representations of images and videos. These methods are often pre-trained on large-scale unlabeled image or video data with specific upstream (*i.e.*, *proxy* or *pretext*) tasks and then fine-tuned to adapt to downstream tasks. Learned representations from unlabeled images

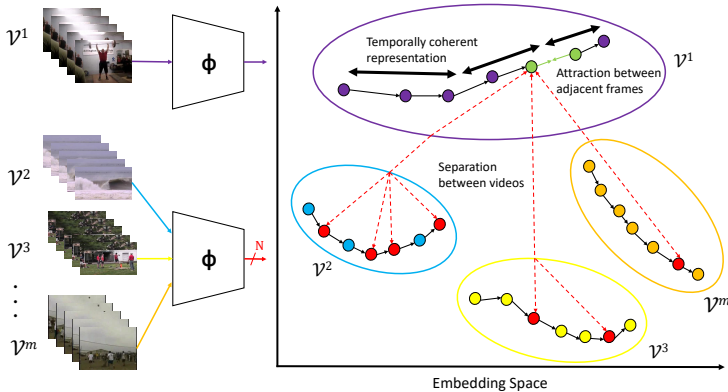


Fig. 1: Overview of *TCE*: *Temporally Coherent Embeddings* for self-supervised video representation learning. We train an embedding function to encode videos such that adjacent frames exist close to each other and videos are separated from one another. At each step relative attraction and separation is achieved by contrasting an anchor frame and those adjacent to  $N$  randomly sampled negative examples from other videos.

have been shown to successfully transfer to multiple downstream tasks such as image classification [2,5,38] and object detection [12,23], in some cases successfully outperforming fully-supervised methods [5]. However, self-supervision from videos is still not very effective for downstream tasks such as action recognition [14] and dense correspondences [8] despite videos being a rich source of self-supervision.

Current state of art approaches for self-supervised representation learning from videos fall into two categories: ranking methods [9,10,22,25,29,50], and predictive methods [14,27,28,36,42,41]. Ranking methods randomly shuffle subsequent frames or clips from a video, and solve *pretext* tasks related to determining the original order. Predictive methods can be grouped into two categories: those that predict a pixel level reconstruction of future frames [27,28,36,42], and those that predict latent representations of future frames in the embedding space [14,41]. However, for both ranking and predictive methods the use of hand-designed *pretext* tasks can lead to shortcomings when transferring the learnt embeddings to downstream tasks. El-Nouby *et al.* [9] and Kim *et al.* [22] demonstrate that trivial solutions and noisy pseudo-labels can hinder the generalisability of ranking approaches to downstream tasks. Pixel-space predictive methods are limited by the need to predict the low-level details of frame pixels [16]. In contrast, predictive methods are designed to predict the embedding of the future frames based on the recent past. However, they are still limited by the fact that the future is not deterministic [14].

Our approach to the problem of self-supervised representation learning from videos is motivated by the question: What properties are desirable in an embedding space for the downstream task of video action recognition? We believe one of

essential properties of learned representations from videos is temporal coherency. High-level visual information in the world changes smoothly and consistently, and we believe that adjacent frames in a learned embedding space should behave in a similar fashion. Inspired by recent advances in self-supervised learning in the image domain [2,5] we introduce *Temporally Coherent Embeddings (TCE)*, a contrastive loss function designed to learn a temporally coherent embedding space from unlabeled videos. Instead of using hand-designed heuristics to implicitly learn coherency by ordering or predicting frames, our approach employs a contrastive loss to explicitly enforce coherency in the embedding space by encouraging similarity in the embeddings of temporally adjacent frames without any labels. Our proxy loss consequently learns an embedding space in which high-level visual information changes in a smooth and gradual fashion over time, leading to improved downstream performance on video action recognition. We summarize our contribution as follows:

- We propose *TCE: Temporally Coherent Embeddings* for self-supervised video representation learning. Our method exploits the structure of video data to explicitly enforce temporal coherency in the embedding, rather than indirectly learning it through ranking or predictive tasks.
- In order to demonstrate the quality of our learned representations, we show state-of-the-art results on the UCF101 action recognition dataset for networks pre-trained using unlabeled videos from UCF101, outperforming all the previous more complex 3D-CNN based networks and highly competitive results against networks pre-trained using the large scale Kinetics400 dataset.

## 2 Related Works

Deep neural networks have shown strong results in computer vision tasks such as image classification, object detection and segmentation by leveraging large, publicly available labeled datasets [4,26,49]. However, the lack of labeled data is a limiting factor in the applicability of deep learning to many target problem domains such as action recognition. Prior work [37] establishes a roughly logarithmic relationship between the quantity of data used for training and the performance of a network; however, labeling data is a time consuming and expensive process. Consequently, a large body of work has emerged which seeks to leverage the huge quantities of unlabelled, publicly available data. These works typically define a *pretext* task for which the supervisory signal to learn a data representation can be obtained without hand-labelling. The learned representation with self-supervision are then fine-tuned to adapt to one or more downstream tasks with a reduced dependence on data quantity.

### 2.1 Self-Supervised Learning from Images

There are many different approaches to learning from unlabeled images which can be categorised into contrastive and generative methods [12]. Generative

methods learn a representation of the data which allows the prediction of missing components of the data. Common examples include predicting a color image from its grey scale counterpart [43,51] and using the reconstruction signal from auto-encoders to produce a self-supervised encoder [33,40,52]. However, as these methods are trained on a per pixel basis, they have been shown to produce features that do not transfer to other downstream tasks very well [52].

Other methods have encouraged higher level features by splitting the training image into a series of patches. For example [6] learns representations by predicting the relative position of two patches within an image, while [31] learns representations by extracting multiple tiles from the training image and shuffling them into one of a number of predefined permutations to make jigsaw puzzles. Other notable approaches have predicted image rotations without reference to the original image [11], and discrimination between a patch taken from a training image and surrogate classes created by applying a family of transformations to that patch [7].

Conversely to generative methods, contrastive approaches build representations by modelling the differences and similarities between two or more inputs. In these methods, negative examples are required to contrast against [2,16,18,32,34,38]. The key differences between generative and contrastive methods is the calculation of the error used for training and its implication on the learned representation. Predictive methods compute the error in the pixel space whereas contrastive methods form a loss term in the embedding space. Contrastive methods tend to be able to learn more abstract, latent representations as a result because pixel level loss functions commonly assume independence between pixels and rely on pixel level details such as colour.

Recently, contrastive methods have been successful in static image representation learning. Approaches in [18] and [2] maximise mutual information (MI) between local and global features, respectively. Mutual information maximisation has featured in numerous unsupervised feature learning approaches [2,16,18,32,38]. Several formulations of MI, including those based on Kullback-Leibler (KL) and Jensen-Shannon (JSD) divergences, have been proposed over the years [3,18,47]. However, recent developments in this area have shown significant performance boosts proportional to the number of negative examples used in training [2,30,38,39]. Processing such numbers of negatives is generally only tractable when employing an approximation of MI such as Noise Contrastive Estimation (NCE) or it's variations [13]. Tian *et al.* [38] propose to learn embeddings by contrasting between different colourspaces of the same image, training a separate network on each colourspace. They also expand their proposed system to different frames of videos. In this case, their optimisation objective is mathematically similar to what we present here. However we train only a single network and consequently present significant improvements on downstream task performance.

## 2.2 Self-Supervised Learning from Video Data

Videos, in contrast to still images, provide a valuable temporal structure that can be leveraged as an additional training signal for self-supervision. Recent SSL approaches for video data can be classified into ranking and predictive methods. Ranking methods learn to solve *pretext* tasks to recover the temporal order of shuffled video frames. Many such approaches [10,29] learn representations by classifying whether or not a series of input frames are presented in chronological order. Lee *et al.* [25] take this approach a step further and, instead, sort sequences of frames as a *pretext* task to learn representations, taking an input of four frames and determining their chronological order. Several methods further extend this method of sequence sorting with 3D CNNs to sort sequences of clips taken from the video instead of sorting single frames [9,22,50]. These methods achieve higher performance on downstream tasks than their 2D CNN predecessors.

Predictive methods can be grouped in two sub-categories, representative and reconstructive. Vondrick *et al.* [41] and Han *et al.* [14] predict latent representations of future video frames similar to the aforementioned generative SSL methods for static images. The 3D-CNN based architecture proposed by Han *et al.* [14] is currently the state of the art for self-supervised representation learning as demonstrated on the task of action recognition for the UCF101 dataset. The high performance and representation ability of 3D CNN architectures, shown in several self-supervised predictive methods and ranking methods, is not without significant computational cost. Han *et al.* [14] note that their model took six weeks to train on the Kinetics400 dataset and four Nvidia P40 GPUs. A number of methods have also attempted to reconstruct future video frames rather than future latent representations [27,28,36,42]. The representation ability of reconstructive methods is constrained by their requirement to predict pixel level details of images. This leaves such methods less likely to model abstract, semantic features and hence less likely to transfer to downstream tasks [14,16].

Several previous methods have also explored the idea of temporal coherency as a signal for self-supervision. Jayaraman *et al.* [20] propose using temporal coherence as an auxiliary signal for semi-supervised learning from videos. Wang *et al.* [45] uses a triplet loss formulation to learn coherence between patches across frames, though they use a kernelized correlation filter [17] to ensure similarity between the positive examples. Sermanet *et al.* [34] also employ a triplet and  $n$ -pair loss formulation to learn video representations. Their approach learns from viewpoints of the same action taken from either different videos or different frames in the same video. Such a constraint on the training data encourages their model to learn viewpoint invariant features for different actions. However their loss formulation contrasts only one negative with the positive pair at any time, which does not leverage the advantages found in using multiple negatives described by [2,30,38,39]. Furthermore their learnt model is trained on only one class of videos and is not tested on diverse action recognition datasets with multiple classes, such as UCF101 [35] or HMDB51 [24]. Conversely, our method leverages multiple negatives from a number of diverse videos on a publicly available dataset. Hence, *TCE* has a wider range of data that could be used. Finally, Isola *et al.* [19] train a

simple classifier to detect whether or not frames taken from a video occur within a given time frame of one another. We show in this work that our method extends previous attempts to use temporal coherency for SSL by leveraging contrastive methods to attract frame embeddings without using a supervised signal or relying on priors such as trackers to assist our selection of positive examples.

### 3 Methodology

We propose a simple framework to learn a temporally coherent embedding space from unlabeled videos. The mathematical formulation of our method, *TCE*: *Temporally Coherent Embeddings* for self-supervised video representation learning, is explained in this section.

#### 3.1 Temporal Coherency Training

The goal of our proposed method, *TCE*, is to explicitly enforce coherency in the embedding space by encouraging similarity in the embeddings of temporally adjacent frames without any labels.

To develop representations which are coherent in time, we seek to learn an embedding function  $f(\cdot)$  which transforms a video frame  $x_t^i$  from pixel-space into a lower dimensional embedding space. We adopt the shorthand notation  $f(x_t^i) := f_t^i$  for the transformed frame.

We define temporal coherency as minimisation of the temporal derivatives of the representations in embedding space. First-order temporal coherence in the embedding space is thus achieved when  $\partial f_t / \partial t \approx 0$ , and can be extended to the  $n^{\text{th}}$  order by requiring  $\partial f_t^n / \partial^n t \approx 0$  [20].

To the first order, coherence is maximised by minimising a distance function  $d(f_{t+1}^i, f_t^i)$  between two temporally adjacent frames in the same video, as  $\partial f_t / \partial t \propto f_{t+1} - f_t$ . A trivial solution to this optimisation goal is apparent: an embedding function which simply maps all inputs to the same point in representation space. To avoid such a trivial solution, a number of existing approaches adopt a contrastive learning paradigm rather than simply minimising  $d(f_{t+1}^i, f_t^i)$ . One such approach is to formulate a triplet loss paradigm that also seeks to maximise distance to some *negative* frame representations [20]. This triplet loss is:

$$\mathcal{L} = \mathbb{E} [d(f_t, f_{t+1}) + \max(\delta - d(f_t, f_n), 0)], \quad (1)$$

where  $\mathbb{E}$  denotes the expectation value, in this case over a set positive pairs of frames.  $f_n$  is the negative frame representation and  $\delta$  is some distance margin which  $d(f_t, f_n)$  should be greater than in order to minimise the loss. In this paradigm, the two temporally adjacent frames are considered positive examples.

Rather than minimise distance between frame representations, an alternative formulation is to maximise a similarity metric between representations,  $s(f_{t+1}, f_t)$ . A similarity-maximising alternative to Equation 1 is to minimise this loss function:

$$\mathcal{L} = -\mathbb{E}[s(f_{t+1}, f_t) - \min(\delta - s(f_t, f_n), 0)] \quad (2)$$

A suitable similarity function is the inner product between  $l_2$  normalized representations:  $s(f_{t+1}, f_t) = f_{t+1}^T f_t$ . This similarity function is minimised when  $f_{t+1} = f_t$ , at which point the distance is also minimised. In the supplementary materials, we show that minimising distance between  $l_2$  normalised features will always increase their inner product at all stages during optimization.

Inspired by other works which show that leveraging multiple negative examples can lead to improved performance on a number of tasks [1,2,16,30], we improve upon the triplet loss in Equation 2 by formulating the task as a binary classification between one positive and  $\mathcal{N}$ , a set of  $N$  negative examples.

Consider a video dataset where each video  $\mathcal{V}^i$  contains  $T^i$  frames  $\{x_1^i, x_2^i, \dots, x_{T^i}^i\}$ . We consider a pair of temporally neighbouring frames from one video as positive examples, and consider all frames from other videos to be negative examples. We sample these negative examples to form a set  $\mathcal{N}$  containing  $N$  frames. We adopt a standard cross-entropy loss in Equation 3 which is minimised when  $s(f_t, f_{t+1})$  is large and  $s(f_t, f_n)$  is small for all  $x_n \in \mathcal{N}$ , as per similar works in [14,30,32].

$$\mathcal{L}_{1^{\text{st}}}(x_{t+1}^i, x_t^i, \mathcal{N}) = -\mathbb{E} \left[ \log \frac{e^{(s(f_t, f_{t+1}))}}{e^{(s_1(f_t, f_{t+1}))} + \sum_{\mathcal{N}} e^{(s(f_t, f_n))}} \right] \quad (3)$$

Minimising this loss function is analogous to training a binary classifier to correctly select the positive example from all negative examples in  $\mathcal{N}$ .

### 3.2 Higher Order Coherency

To the first order, the coherency objective will encourage neighbouring video frames to cluster in representation space because it penalises large distances between frames in the embedding space. Additional temporal structure in the embeddings can be captured through higher order coherency. For example, a second-order coherency objective is one which, in addition to minimizing the first-order derivative of embedding vectors with respect to time, has the optimization goal of setting  $\partial^2 f_t / \partial t^2 \approx 0$ . This optimization goal is accomplished when  $f_{t+2} - f_{t+1} \approx f_{t+1} - f_t$ .

By extending the coherency objective to second-order the optimization goal is changed from clustering temporally adjacent frame embeddings to also clustering the differences between those embeddings. Clustering the differences between embeddings ensures that the direction that the embeddings travel does not significantly vary over short time periods, resulting in trajectories that are more smooth. The second-order cross-entropy loss is:

$$\mathcal{L}_{2^{\text{nd}}} = -\mathbb{E} \left[ \log \frac{e^{(s_2(f_t, f_{t+1}, f_{t+2}))}}{e^{(s_2(f_t, f_{t+1}, f_{t+2}))} + \sum_{\mathcal{N}_2} e^{(s_2(f_t, f_{t+1}, f_n))}} \right], \quad (4)$$

where  $s_2(f_{t+2}, f_{t+1}, f_t)$  is a modified version of the similarity function acting on the differences between the three temporally adjacent frames. That is,  $s_2(f_t, f_{t+1}, f_{t+2}) = s(f_{t+1} - f_t, f_{t+2} - f_{t+1})$ . We also stress that the negative examples used in calculating the second-order cross-entropy loss are distinct from those used when calculating first-order loss. Most notably, the second-order coherency objective seeks to cluster differences between embeddings rather than the embeddings themselves and so sampling negative examples from other videos does not provide sufficiently difficult negative examples to learn from. For this reason, negative samples in  $\mathcal{N}_2$  are sampled within the same video as the positives.

The coherency objective described can be extended to higher order derivatives trivially by defining the appropriate similarity function. In the general case, the similarity function for the  $n$ th order derivative can be recursively defined as  $s_n(f_{t+n}, \dots, f_t) = s_{n-1}(f_{t+n} - f_{t+n-1}, \dots, f_{t+1} - f_t)$ .

### 3.3 Leveraging Multiple Negative Examples with Noise Contrastive Estimation (NCE)

For large numbers of negative examples, calculating the normalization factor for the full softmax distribution in Equation 3 can prove computationally intractable [30]. Noise Contrastive Estimation (NCE) [13] is a computationally efficient means of estimating unnormalized statistical models and performing logistic regression to discriminate between observed data and a noise distribution. In this case, discriminating between the positive and negative examples.

The posterior probability that a given pair of embeddings belong to the data distribution  $C$  – that is, they are a pair of positive examples – is:

$$P(C|x_1, x_2) = \frac{P(x_2|x_1)}{P(x_2|x_1) + NP_n(x_2|x_1)}, \quad (5)$$

where  $P(x_2|x_1)$  is the probability that  $x_2$  is a positive example from the data distribution given  $x_1$ , and  $P_n(x_2|x_1)$  is the probability that it is a negative example taken from the noise distribution. Any noise distribution can be chosen so long as it is computationally easy to sample from and does not assign zero probability to any frame  $x_2$ . Akin to [30,38], we choose a uniform distribution such that  $P_n(x_2|x_1) = 1/N \ \forall x_2 \in \mathcal{N}$ . The similarity function  $s_1$  can be converted to a probability describing the probability of a second frame  $x_2$  being a positive for the given frame  $x_1$ , by exponentiating and normalizing:

$$P(x_2|x_1) = \frac{e^{(s_1(f_1, f_2))}}{e^{(s_1(f_1, f_2))} + \sum_{\mathcal{N}} e^{(s_1(f_1, f_n))}} \quad (6)$$

With NCE, the posterior probability in Equation 5 is instead estimated from the unnormalized similarity distribution from the model, so that it can instead be written:

$$P(C|x_1, x_2) = \frac{e^{s(f_1, f_2)}}{e^{s(f_1, f_2)} + NP_n(x_2|x_1)} \quad (7)$$

The NCE based approximation of the optimization goal of the model can be adapted from Equation 3. It is simple to minimise the negative log-posterior probability in Equation 7.

$$\mathcal{L}_{NCE} = -\mathbb{E}_{x, x_p} \left\{ [\log P(C|x; x_p)] + N\mathbb{E}_{x_n \in \mathcal{N}} \left[ \log P(\tilde{C}|x; x_n) \right] \right\}, \quad (8)$$

where  $P(\tilde{C}|x; x_n) = 1 - P(C|x; x_n)$  is the probability of correctly classifying a sample from the noise distribution.

## 4 Experimental Results

In this section we evaluate the performance of our proposed method in a number of ways. We trained a classification network on an action recognition task using the self-supervised learned representation. We investigate the effect that training with multiple negatives has on results, in addition to the method of network initialization, and the effects of enforcing higher order temporal coherency. We also directly evaluate the features that our method produces against those from other training methods including ImageNet pretraining.

### 4.1 Dataset

*TCE* is a generalised method of learning robust representations of video data. Here we focus on the task of video action recognition. Specifically, we train and evaluate *TCE* on the UCF101 dataset [35]. Containing 101 human action classes and 13,000 videos, UCF101 is a common benchmark dataset for both action recognition as well as many self-supervised approaches. Three different train/test splits were released with the data. Aligning with self-supervised methods [50,29] and [9], we train and evaluate on the first train/test split.

### 4.2 Self-Supervised Training

We train an embedding function on the UCF101 dataset without labels to learn robust video representations. The network architecture on which we train is ResNet-50 [15]. We initialize the network with random weights and train for a total of 9 epochs with 4 Tesla-V100 GPUs. Training is completed using a stochastic gradient descent optimiser and batch size of 100. Initially a learning rate of 0.03 is used and reduced by a factor of 10 after 5 epochs. Positive examples are taken by sampling two adjacent video frames from the dataset, and each frame in the dataset is used as a positive example once per epoch. During training, frames are resized so that the shortest side is 256 pixels while preserving image scale, and are then randomly cropped to a  $224 \times 224$  window. Random horizontal flipping is also employed.

$N_1 = 2048$  negative samples used in optimizing first order coherency are drawn from randomly selected videos in the dataset, excluding the video from which positive examples were drawn. Our rationale behind this sampling regime

is that by sampling from videos other than the positive embeddings, we ensure our negatives are significantly different in appearance. For higher order coherency experiments,  $N_2 = 100$  negative examples are sampled from within the same video as the positive examples are drawn.  $N_2$  is significantly smaller than  $N_1$  as the number of frames available in a single video is significantly smaller than those in the rest of the dataset.

Inspired by Wu *et al.* [48], we maintain a memory bank to store embeddings for each frame in the dataset to efficiently retrieve noisy samples without re-computing their embeddings. The memory bank is dynamically updated with the new embeddings on every forward pass of the network.

### 4.3 Action Recognition

**Training** We benchmark the quality of our learned embedding function by finetuning our network for action recognition on the UCF101 [35] dataset, which contains in excess of 13,000 videos of 101 action classes. Following [29,9,50] we perform experiments and report on the first test/train split of the dataset.

During training, we replace the final fully connected layer of our pretrained network with another fully-connected layer of 101 nodes, using the ReLu activation function. We employ the stack-of-differences video-clip encoder introduced by [10]. Six neighbouring frames are taken from the video to produce an input with size  $224 \times 224 \times 15$  by resizing each image to  $224 \times 224$  pixels and taking the differences between the five neighbouring pairs of frames. The convolutional layers of our pretrained network are duplicated five times in order to allow the 15-channel input to be fed through the network.

During evaluation, nineteen evenly-spaced blocks of six frames are taken from each video. Softmax outputs on each block of frames are averaged, and the highest average value is the classification output for the video. We report results for the highest scoring epoch during training for all our experiments. The network is trained using 4 Tesla-V100 GPUs and stochastic gradient descent for 600 epochs with a learning rate of 0.05 that is decayed by a factor of 10 after 350 epochs.

**Comparison to State-of-the-Art** The results of our training method are compared against other state-of-the-art results in Table 1. We achieve higher Top-1 classification accuracy with pretraining on the UCF101 dataset than any other approach in the literature which trains on the same dataset, as far as we are aware. Notably this is irrespective of network architecture and our approach implemented on ResNet50 outperforms Video Clip Ordering [50] – which uses 3D ResNet18 as the network backbone – by 3.8% despite being implemented on a 2D convolutional network.

Our approach also surpasses the vast majority of the those pre-trained on the Kinetics400 dataset despite using a significantly smaller dataset for pre-training. The only approach in the literature which surpasses our result is Dense Predictive Coding (DPC) [14] which is both trained on the Kinetics400 [4] - which contains

Table 1: Top-1 accuracy performance for action recognition task on UCF101 dataset. \* Network architecture using stack-of-differences for downstream training. \*\* Two networks which do not share weights. <sup>+</sup> Results reported on train/test split 1 of UCF101.

Method	Backbone	2D-CNN	Pre-Training	UCF101 (%)
Motion & Appearance [44]	C3D	✗	Kinetics400	61.2
3DRotNet [21]	3D ResNet-18	✗	Kinetics400	62.9
3DCubicPuzzles [22]	3D ResNet-18	✗	Kinetics400	65.8
DPC [14]	3D ResNet-18	✗	Kinetics400	68.2
DPC [14]	3D ResNet-34	✗	Kinetics400	<b>75.7</b>
Shuffle and Learn [29] <sup>+</sup>	AlexNet	✓	UCF101	50.9
VideoGAN [42]	C3D	✗	UCF101	52.1
Arrow of time [46]	AlexNet	✓	UCF101	55.3
OPN [10]	AlexNet	✓	UCF101	56.3
CMC [38]	CaffeNet $\times 2^{**}$	✓	UCF101	59.1
Motion & Appearance [44]	C3D	✗	UCF101	58.8
O3N [10]	AlexNet <sup>*</sup>	✓	UCF101	60.3
DPC [14]	3D ResNet-18	✗	UCF101	60.6
Skip-Clip [9] <sup>+</sup>	3D ResNet-18	✗	UCF101	64.4
Video Clip Ordering [50] <sup>+</sup>	R3D	✗	UCF101	64.9
<b>TCE (Ours)<sup>+</sup></b>	ResNet-50 <sup>*</sup>	✓	UCF101	<b>68.7</b>

306K video clips, as opposed to only 13K for UCF - and employs the extremely high capacity 3D ResNet-34 network architecture. Notably, DPC’s network took six weeks to train [14], while our approach completed pre-training and fine-tuning on action recognition within four days. We plan to explore use of Kinetics400 in future work to demonstrate the scalability of our method to larger datasets.

#### 4.4 Analysis of Results

In this section we detail experiments to analyse the performance of *TCE*. We compare our results to random network initialization and ImageNet pretraining in order to gauge how our choice of network architecture and loss function impacts the performance of the downstream action-recognition task, and also investigate how changing the number of negatives sampled affects performance. Finally, we investigate how higher order coherency objectives affect the results achieved.

**Comparison to Random Initialization** Table 2 details the performance achieved by our network on the action recognition task when trained from randomly initialized weights, ImageNet pretrained weights, and our self-supervised representation, *TCE*.

We report a 14.9% improvement over training from random weights and achieve 88.5% of the ImageNet pretraining baseline. This significant improvement demonstrates that our embedding space learns features which generalise well to the task of action recognition and further validates *TCE* against the standard

Table 2: Top-1 accuracy performance for action recognition task on UCF101 dataset for different initialization methods of our network.

Initialization	UCF101
Random	59.82
ImageNet	77.69
<i>TCE</i> (Ours)	68.75

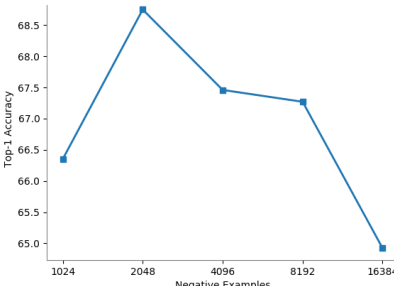


Fig. 2: Top-1 Accuracy on UCF101 action recognition task versus the number of negative examples used during training.

approach of full supervision. Notably, the combination of ResNet50 and stack-of-differences in the downstream task achieves 59.82% accuracy after training with randomly initialized weights, well above results on AlexNet quoted in [10, 29, 46].

**Investigating the Effects of Negative Samples** We also investigated how the number of negative examples sampled when calculating first-order cross-entropy loss affect performance on the action recognition downstream task. Fig. 2 illustrates the relationship between the number of negative examples sampled, and the Top-1 classification accuracy on the action recognition classification task. We found that increasing the number of negatives examples used improved Top-1 Accuracy up to a value of 2048 negatives, after which adding additional negatives caused performance to decline.

**Investigating the Effects of High-Order Coherency Objectives** We investigate the effect of implementing a higher-order loss term to *TCE*, with results presented in Table 3. The First + Second Order result is trained on a total loss which is the sum of the first-order coherency loss introduced in Equation 3 with the second-order loss introduced in Equation 4.

Table 3: Action recognition performance on UCF101 when training *TCE* with and without enforcing a second-order coherency.

Method	UCF101
First Order Only	67.46
First + Second Order	66.35

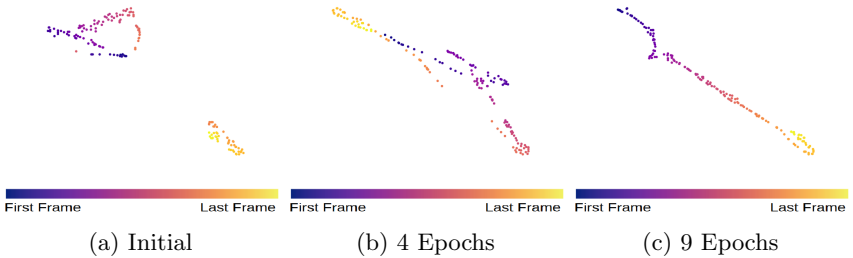


Fig. 3: t-SNE visualisation of frame embeddings produced by our network on one video in the UCF101 validation set before training (a); after training for four epochs (b); and after nine epochs (c).

In both training cases, we pretrain on UCF101 with  $N_1 = 4096$  and  $N_2 = 100$  negatives when calculating first and second-order loss terms respectively.  $N_2$  is lower than  $N_1$  as the number of frames available in a single video is significantly smaller than those in the rest of the dataset.

We found that implementing a higher order coherency term to the loss function resulted in diminished downstream performance for action recognition, compared to simply training with first-order loss. We believe that this is because the within-video negative examples are too similar to the positive examples and act as noise when learning, hindering the overall performance. Other methods which leverage negative examples from within-video introduce a temporal buffer to ensure that negative examples are temporally distant to the positive examples and so are easier for the network to distinguish during training. We have included a similar study in the supplementary materials.

#### 4.5 Evaluating Our Embeddings

In this section we qualitatively evaluate the effectiveness of *TCE* in creating a temporally coherent embedding space. We visualise our embedding space by using t-SNE to reduce our frame embeddings to two dimensions, so that each point in the graph represents a single frame. We use a color map to show the temporal order of frames for figures containing only a single video.

**Coherence during Training** Fig. 3 visualises the evolution of our embedding space over the course of training. Our training increases the temporal coherency of the embedding space across epochs, from almost no coherency for random weights in (a) to partial coherency at four epochs in (b) and very strong coherency at nine epochs in (c). t-SNE is used to reduce the dimensionality of the embeddings for plotting. Each point on the graph represents a different frame of the video. During training, our method successfully learns an embedding function which produces temporally coherent frame embeddings from a single video.

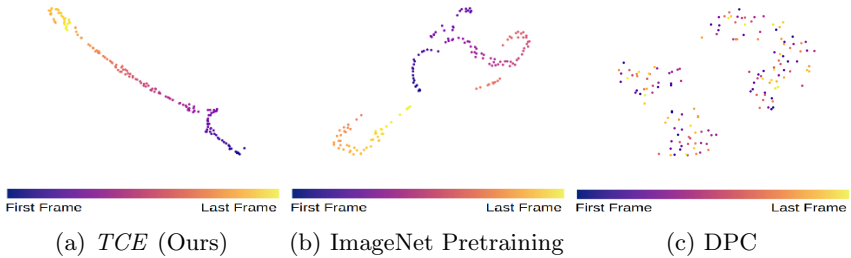


Fig. 4: Comparison between frame embedding on one video (Bowling class) in UCF101 with *TCE* (a); ImageNet pretraining (b); and DPC [14] (c).

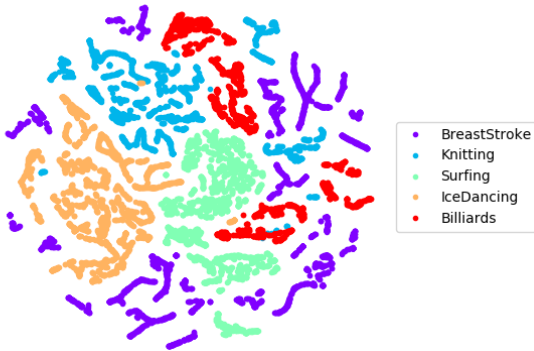


Fig. 5: t-SNE visualisation of UCF101 frame embeddings produced with *TCE*. Ten random videos from five classes in the UCF101 validation set are represented.

**Comparison to other methods** Figure 4 compares visualisations of our embedding space against an ImageNet pre-trained checkpoint and DPC [14]. Implementation details for how we obtained the t-SNE for DPC can be found in the supplementary materials. Our method demonstrates significantly better coherency than both ImageNet and DPC, with frames over time forming a coherent path with no major discontinuities.

**Class Clustering** Fig. 5 plots ten videos from five classes taken from the UCF101 validation set, with each point in the t-SNE representing a single frame. We observe a clear separation between videos in the embedding space, and strong separation between different action classes.

## 5 Conclusion

In this paper, we have presented an approach to learn embeddings from unlabelled videos, *TCE: Temporally Coherent Embeddings*. Specifically, we train our model

in a self-supervised manner by leveraging the temporal information embedded in video data and enforcing coherency in the embedding space. At each step relative attraction and separation is achieved by contrasting an anchor frame and those adjacent to  $N$  randomly sampled negative examples from other videos. We applied the learned representation to the downstream task of video action recognition. Our method outperforms previous 2D-CNN self-supervised learning approaches by 8%, using UCF101. We achieve 68.7% accuracy, despite using a significantly smaller dataset for pre-training. Most importantly, our results reveal that our model delivers competitive generalization results without the complexity of 3D-CNN network architecture. We believe this shows that explicitly enforcing temporal embedding coherency between nearby frames is a powerful learning signal for action recognition, resulting in models that are required smaller computational training capacity and are faster at inference time. For future work we plan on investigating transfer learning of pre-trained *TCE* for downstream tasks that require a level of temporal understanding, such as robotic perception.

## References

1. Arora, S., Khandeparkar, H., Khodak, M., Plevrakis, O., Saunshi, N.: A theoretical analysis of contrastive unsupervised representation learning. arXiv preprint arXiv:1902.09229 (2019)
2. Bachman, P., Hjelm, R.D., Buchwalter, W.: Learning representations by maximizing mutual information across views. arXiv preprint arXiv:1906.00910 (2019)
3. Becker, S.: An information-theoretic unsupervised learning algorithm for neural networks. University of Toronto (1992)
4. Carreira, J., Zisserman, A.: Quo vadis, action recognition? a new model and the kinetics dataset (2017)
5. Chen, T., Kornblith, S., Norouzi, M., Hinton, G.: A simple framework for contrastive learning of visual representations. arXiv preprint arXiv:2002.05709 (2020)
6. Doersch, C., Gupta, A., Efros, A.A.: Unsupervised visual representation learning by context prediction. In: Proceedings of the IEEE International Conference on Computer Vision. pp. 1422–1430 (2015)
7. Dosovitskiy, A., Fischer, P., Springenberg, J.T., Riedmiller, M., Brox, T.: Discriminative unsupervised feature learning with exemplar convolutional neural networks (2014)
8. Dwibedi, D., Aytar, Y., Tompson, J., Sermanet, P., Zisserman, A.: Temporal cycle-consistency learning. In: Proceedings of the IEEE Conference on Computer Vision and Pattern Recognition. pp. 1801–1810 (2019)
9. El-Nouby, A., Zhai, S., Taylor, G.W., Susskind, J.M.: Skip-clip: Self-supervised spatiotemporal representation learning by future clip order ranking. arXiv preprint arXiv:1910.12770 (2019)
10. Fernando, B., Bilen, H., Gavves, E., Gould, S.: Self-supervised video representation learning with odd-one-out networks. In: Proceedings of the IEEE conference on computer vision and pattern recognition. pp. 3636–3645 (2017)
11. Gidaris, S., Singh, P., Komodakis, N.: Unsupervised representation learning by predicting image rotations. arXiv preprint arXiv:1803.07728 (2018)
12. Goyal, P., Mahajan, D., Gupta, A., Misra, I.: Scaling and benchmarking self-supervised visual representation learning. arXiv preprint arXiv:1905.01235 (2019)

13. Gutmann, M., Hyvärinen, A.: Noise-contrastive estimation: A new estimation principle for unnormalized statistical models. In: Proceedings of the Thirteenth International Conference on Artificial Intelligence and Statistics. pp. 297–304 (2010)
14. Han, T., Xie, W., Zisserman, A.: Video representation learning by dense predictive coding. In: Proceedings of the IEEE International Conference on Computer Vision Workshops. pp. 0–0 (2019)
15. He, K., Zhang, X., Ren, S., Sun, J.: Deep residual learning for image recognition. In: Proceedings of the IEEE conference on computer vision and pattern recognition. pp. 770–778 (2016)
16. Hénaff, O.J., Razavi, A., Doersch, C., Eslami, S., Oord, A.v.d.: Data-efficient image recognition with contrastive predictive coding. arXiv preprint arXiv:1905.09272 (2019)
17. Henriques, J.F., Caseiro, R., Martins, P., Batista, J.: High-speed tracking with kernelized correlation filters. IEEE transactions on pattern analysis and machine intelligence **37**(3), 583–596 (2014)
18. Hjelm, R.D., Fedorov, A., Lavoie-Marchildon, S., Grewal, K., Bachman, P., Trischler, A., Bengio, Y.: Learning deep representations by mutual information estimation and maximization. arXiv preprint arXiv:1808.06670 (2018)
19. Isola, P., Zoran, D., Krishnan, D., Adelson, E.H.: Learning visual groups from co-occurrences in space and time. arXiv preprint arXiv:1511.06811 (2015)
20. Jayaraman, D., Grauman, K.: Slow and steady feature analysis: higher order temporal coherence in video. In: Proceedings of the IEEE Conference on Computer Vision and Pattern Recognition. pp. 3852–3861 (2016)
21. Jing, L., Yang, X., Liu, J., Tian, Y.: Self-supervised spatiotemporal feature learning via video rotation prediction (2018)
22. Kim, D., Cho, D., Kweon, I.S.: Self-supervised video representation learning with space-time cubic puzzles. In: Proceedings of the AAAI Conference on Artificial Intelligence. vol. 33, pp. 8545–8552 (2019)
23. Kolesnikov, A., Zhai, X., Beyer, L.: Revisiting self-supervised visual representation learning. arXiv preprint arXiv:1901.09005 (2019)
24. Kuehne, H., Jhuang, H., Garrote, E., Poggio, T., Serre, T.: Hmdb: a large video database for human motion recognition. In: 2011 International Conference on Computer Vision. pp. 2556–2563. IEEE (2011)
25. Lee, H.Y., Huang, J.B., Singh, M., Yang, M.H.: Unsupervised representation learning by sorting sequences. In: Proceedings of the IEEE International Conference on Computer Vision. pp. 667–676 (2017)
26. Liu, Y., Wang, Y., Wang, S., Liang, T., Zhao, Q., Tang, Z., Ling, H.: Cbnet: A novel composite backbone network architecture for object detection. arXiv preprint arXiv:1909.03625 (2019)
27. Lotter, W., Kreiman, G., Cox, D.: Deep predictive coding networks for video prediction and unsupervised learning. ICLR (2017)
28. Mathieu, M., Courville, C., LeCun, Y.: Deep multi-scale video prediction beyond mean square error. ICLR (2016)
29. Misra, I., Zitnick, C.L., Hebert, M.: Shuffle and learn: unsupervised learning using temporal order verification. In: European Conference on Computer Vision. pp. 527–544. Springer (2016)
30. Mnih, A., Kavukcuoglu, K.: Learning word embeddings efficiently with noise-contrastive estimation. In: Advances in neural information processing systems. pp. 2265–2273 (2013)

31. Noroozi, M., Favaro, P.: Unsupervised learning of visual representations by solving jigsaw puzzles. In: European Conference on Computer Vision. pp. 69–84. Springer (2016)
32. Oord, A.v.d., Li, Y., Vinyals, O.: Representation learning with contrastive predictive coding. arXiv preprint arXiv:1807.03748 (2018)
33. Pathak, D., Krahenbuhl, P., Donahue, J., Darrell, T., Efros, A.A.: Context encoders: Feature learning by inpainting. In: Proceedings of the IEEE conference on computer vision and pattern recognition. pp. 2536–2544 (2016)
34. Sermanet, P., Lynch, C., Chebotar, Y., Hsu, J., Jang, E., Schaal, S., Levine, S., Brain, G.: Time-contrastive networks: Self-supervised learning from video. In: 2018 IEEE International Conference on Robotics and Automation (ICRA). pp. 1134–1141. IEEE (2018)
35. Soomro, K., Zamir, A.R., Shah, M.: Ucf101: A dataset of 101 human actions classes from videos in the wild. arXiv preprint arXiv:1212.0402 (2012)
36. Srivastava, N., Mansimov, E., Salakhudinov, R.: Unsupervised learning of video representations using lstms. In: International conference on machine learning. pp. 843–852 (2015)
37. Sun, C., Shrivastava, A., Singh, S., Gupta, A.: Revisiting unreasonable effectiveness of data in deep learning era. In: Proceedings of the IEEE international conference on computer vision. pp. 843–852 (2017)
38. Tian, Y., Krishnan, D., Isola, P.: Contrastive multiview coding. arXiv preprint arXiv:1906.05849 (2019)
39. Tschannen, M., Djolonga, J., Rubenstein, P.K., Gelly, S., Lucic, M.: On mutual information maximization for representation learning. arXiv preprint arXiv:1907.13625 (2019)
40. Vincent, P., Larochelle, H., Bengio, Y., Manzagol, P.A.: Extracting and composing robust features with denoising autoencoders. In: Proceedings of the 25th international conference on Machine learning. pp. 1096–1103 (2008)
41. Vondrick, C., Pirsiavash, H., Torralba, A.: Anticipating visual representations from unlabeled video. In: Proceedings of the IEEE Conference on Computer Vision and Pattern Recognition. pp. 98–106 (2016)
42. Vondrick, C., Pirsiavash, H., Torralba, A.: Generating videos with scene dynamics. In: Advances in neural information processing systems. pp. 613–621 (2016)
43. Vondrick, C., Shrivastava, A., Fathi, A., Guadarrama, S., Murphy, K.: Tracking emerges by colorizing videos. In: Proceedings of the European Conference on Computer Vision (ECCV). pp. 391–408 (2018)
44. Wang, J., Jiao, J., Bao, L., He, S., Liu, Y., Liu, W.: Self-supervised spatio-temporal representation learning for videos by predicting motion and appearance statistics (2019)
45. Wang, X., Gupta, A.: Unsupervised learning of visual representations using videos. In: Proceedings of the IEEE International Conference on Computer Vision. pp. 2794–2802 (2015)
46. Wei, D., Lim, J.J., Zisserman, A., Freeman, W.T.: Learning and using the arrow of time. In: Proceedings of the IEEE Conference on Computer Vision and Pattern Recognition. pp. 8052–8060 (2018)
47. Wiskott, L., Sejnowski, T.J.: Slow feature analysis: Unsupervised learning of invariances. Neural computation **14**(4), 715–770 (2002)
48. Wu, Z., Xiong, Y., Yu, S., Lin, D.: Unsupervised feature learning via non-parametric instance-level discrimination. arXiv preprint arXiv:1805.01978 (2018)
49. Xie, Q., Hovy, E., Luong, M.T., Le, Q.V.: Self-training with noisy student improves imagenet classification. arXiv preprint arXiv:1911.04252 (2019)

50. Xu, D., Xiao, J., Zhao, Z., Shao, J., Xie, D., Zhuang, Y.: Self-supervised spatiotemporal learning via video clip order prediction. In: Proceedings of the IEEE Conference on Computer Vision and Pattern Recognition. pp. 10334–10343 (2019)
51. Zhang, R., Isola, P., Efros, A.A.: Colorful image colorization. In: European conference on computer vision. pp. 649–666. Springer (2016)
52. Zhang, R., Isola, P., Efros, A.A.: Split-brain autoencoders: Unsupervised learning by cross-channel prediction. In: Proceedings of the IEEE Conference on Computer Vision and Pattern Recognition. pp. 1058–1067 (2017)

## 6 Supplementary Material

In this section we provide appendices to supplement the material of the main paper. Appendix A contains the proof that minimising the distance between  $l_2$  normalized vectors always increases the inner product. Appendix B contains a study on the impact using a margin around our anchor positive to exclude frames from consideration for negative examples and Appendix C outlines the method we used to obtain the t-SNE of Dense Predictive Coding [14] in Figure 4.

### 6.1 Appendix A: Proof that minimising distance between $l_2$ normalised vectors increases inner product

This section provides proof that any optimisation task which maximises the inner product of two  $l_2$  normalized vectors will also minimise distance between those points. The  $l_2$  distance between two  $l_2$  normalized vectors  $u$  and  $v$  can be written as a function of the inner product as follows:

$$\begin{aligned} d_{l_2}^2(u, v) &= \|u - v\|^2 \\ &= u^T u + v^T v - 2u^T v \\ &= 2(1 - u^T v) \end{aligned} \tag{9}$$

The change in distance with respect to the inner product is then:

$$\frac{\partial d_{l_2}}{\partial u^T v} = -\sqrt{\frac{1}{2(1 - u^T v)}} \tag{10}$$

Note that this derivative is always negative, meaning distance monotonically decreased as the inner product increases. Thus an optimisation goal which maximises inner product between  $l_2$  normalized vectors is equivalent to one which minimises distance.

### 6.2 Appendix B: Temporal Buffer in second order coherency

Inspired by [34], we experiment with adding a temporal buffer around our anchor positive when training with second order coherency. Video frames within a margin of  $m$  frames of the anchor positive are excluded from the pool of potential negatives when randomly sampling in-video negative examples for second order coherency. We implemented a margin value of 10 frames which resulted a drop in performance of roughly 2% on action recognition task. We hypothesise that this is due to the fact that [34] uses a triplet loss where the location of a single negative example used has a significant impact on the success of their training. However, as our method uses 100 negative examples sampled from within the video, our performance is more heavily impacted by reducing our pool of potential negative examples than it is by any potential improvement of the quality of the negative examples. We plan to further explore alternative second-order negative sampling methods in our future work.

### 6.3 Appendix C: Dense Predictive Coding (DPC) t-SNE

To create the t-SNE plot from the embeddings in DPC [14], we took the pretrained weights of the 3D-Resnet-34 model learned on  $224 \times 224$  pixel frames in the Kinetics400 dataset<sup>4</sup>.

For every frame in the video that is being visualised, we take a sequence of 25 frames with a temporal stride of 3. Thus the entire sequence spans 73 total frames (the starting frame plus 24 additional frames which are each three frames apart). From this sequence of 25, five non-overlapping blocks of five frames are created and input to the encoder function  $f(\cdot)$ . The five output feature maps are subsequently input to the aggregator function  $g(\cdot)$  which outputs a single feature map with size  $(1 \times 7 \times 7 \times 256)$ . Finally, the feature map is average-pooled to create a single feature vector of size  $1 \times 256$  which can then be further reduced via t-SNE for visualisation on a two-dimensional plot.

This is the same process used to create the t-SNE plot in DPC paper [14], but rather than only show one point per video we visualise the representations of all sequences of frames in the video to identify any temporal coherency that may arise from the training method in DPC. If there are  $T^i$  frames in the video  $\mathcal{V}^i$  being visualised, the t-SNE plot will include  $T^i - 72$  points.

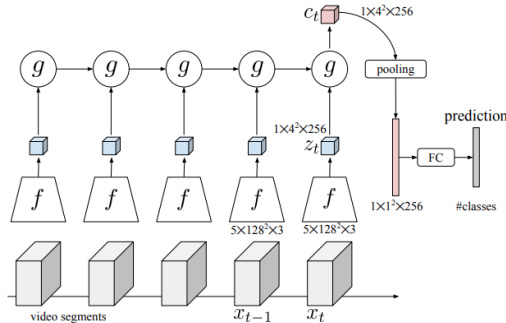


Fig. 6: Network architecture for DPC, taken from [14].

<sup>4</sup> Available at <https://github.com/TengdaHan/DPC>